Modelling of a traditional bow and arrow - Material modelling and dynamic simulation

G. Baumann[1], G. Schickhofer[2], S. Zimmer[2], F. Feist[1]

[1]Vehicle Safety Institute (VSI), Graz University of Technology, AUT
[2]Institute of Timber Engineering and Wood Technology, Graz University of Technology, AUT

1 Abstract

Traditional bow-making is a sophisticated craftsmanship in which the interacting materials are pushed to its limits. The present study deals with a single-piece-recurve bow made of bamboo, carbon fiber, glass fiber and laminated densified wood. In this bow the limbs are rigidly connected to the grip, which leads to stress concentrations in the transition regions. In some cases, these stress concentrations caused delamination. The purpose of this paper was to study the mechanics of the bow and to understand the failure mechanism that led to the delamination problems. The bow and arrow was modelled in LS-DYNA. Beam elements were used for the bow string and the arrow, shell elements for the composite limbs and solid elements for the grip. ***Mat_composite_damage** in combination with ***part_composite** was used for modelling the composite structure of the limbs. The simulation covered multiple phases: bracing (i.e. engaging the bow string and pre-straining the bow), nocking (setting the arrow in the bow), spanning (pulling back the string) and releasing the string. The numerical model was validated against dynamic arrow launching and vibration tests and static tests in terms of brace height (distance between grip and string), deformation, spanning characteristics and string force. The dynamic simulations showed the archer's paradox (bending of arrow when released) very nicely. Eventually the stresses in the grip and in the bonded joints between the individual plies of the composite shell were evaluated and compared against the technical properties (established in experimental tests) of the adhesives. The study showed that the delamination problem was caused by an adhesive failure due to the high stress level perpendicular to the lamina layers (transverse tension). Based on this model minor design changes can be made to prevent delamination failure in future bow designs but also studying and improving the system as a whole.

2 Introduction

Over the course of many thousands' years of archery development a great variety of different designs arose around the globe. Despite the diversity regarding to shape, size, materials or even the principle of operation, the basic components are always identical.

2.1 Definition of term

A bow basically consists of a grip, an upper and lower limb and a bowstring, which is shown in Fig. 1. The limbs are named after the way the bow is held when used. While the lower limbs are facing to the ground the upper limbs show to the sky. The ends of the limbs are connected to each other with the bowstring so that the system is in a pre-strained state. Additional energy for accelerating the arrow is stored in the limbs by drawing the bowstring back to its anchor point, which is standardized 711 mm (28 inches) away from the grip. The limbs which are simply cantilever beams are stressed primarily on bending. In most modern bows the grip is significantly heavier and stiffer than the two limbs. This is due to the fact that a mass concentration in the area were the archer is holding the bow, reduces the shock loading when the arrow is released. On the other hand, the limbs of the bow have to be as light weight as possible so that most of the energy which is stored in the bow goes into the kinetic energy of the arrow.

Fig.1: Components of a traditional single-piece-recurve bow

2.2 Composite structure

To provide light weight limbs natural and/or artificial fiber composite laminate is used in most modern bows. The present limb structure consists of carbon fiber laminate [1] on the tension side, glass fiber laminate [2] on the compression side and bamboo lamella [3] as well as carbon fiber tissue to form the core (see Fig. 2). Except for the carbon fiber tissue all the used materials feature a unidirectional structure. That gives the bow a relatively high stiffness in longitudinal direction relative to its mass. The grip has to be very heavy in relation to the limbs. Therefore, laminated densified wood is used for the purpose. It is a special wood material which consists of beech veneer soaked in phenolic resin. The prepared veneer stripes are densified at a pressure of about 20 – 30 MPa at a temperature of 100 – 150 °C [4]. As a result, the wood product has a density of 1400 kg/m^3 which is about twice as high as the source material while increasing the strength and stiffness and retaining the aesthetics.

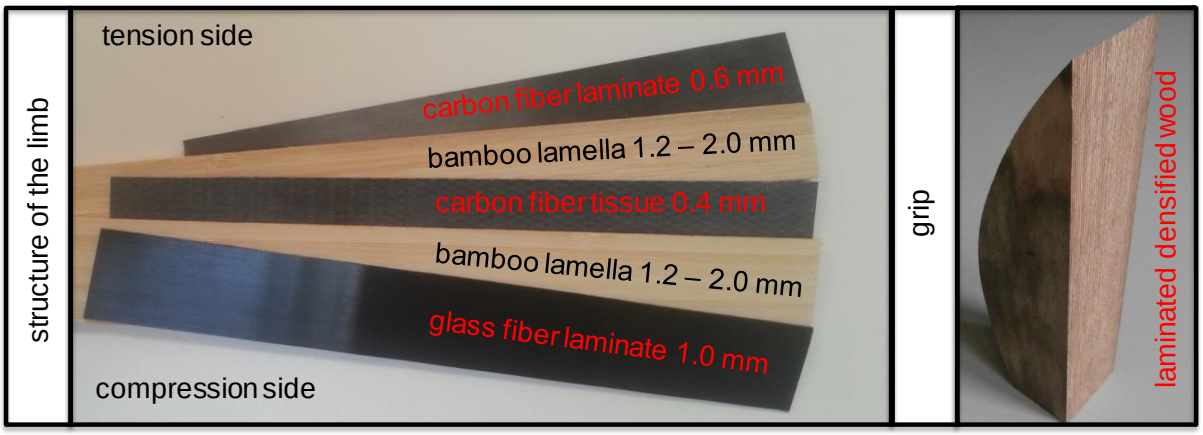

Fig.2: Layer structure of the bow limbs (left) and material of the bow grip (right)

2.3 Problem

In the bow under study, the limbs' tension lamella run over the whole grip (i.e. upper and lower limb are connected). In some bows a delamination failure occurred in the adhesive joint between the grip and the carbon fiber tissue layer, as shown in Fig. 3. According to the manufacturer each delamination failure was located in the area of the grip which features a rounded inward recess.

Fig.3: Delamination failure in the bow grip between the wood handle and the lamellar structure of the limbs

3 Methodical approach

To analyze and understand the failure mechanism that led to the delamination problem a numerical model of the bow was created. As a basis for the development of the numerical model several experiments were conducted.

3.1 Experimental tests

The experiments included material characterization tests to determine the properties of the used adhesive at different load conditions. Afterwards the bow model was validated against quasi-static loading and dynamic unloading tests.

3.1.1 Material characterization / adhesive tests

The adherents (refer to chapter 2.2) are glued with the epoxy resin EA-40 [5].
To determine the mechanical properties of the epoxy resin in combination with its adherents tensile opening tests (mode I) and in plane shear tests (mode II) were conducted (see Fig. 4). The thickness of the adhesive layer was about 0.15 mm.

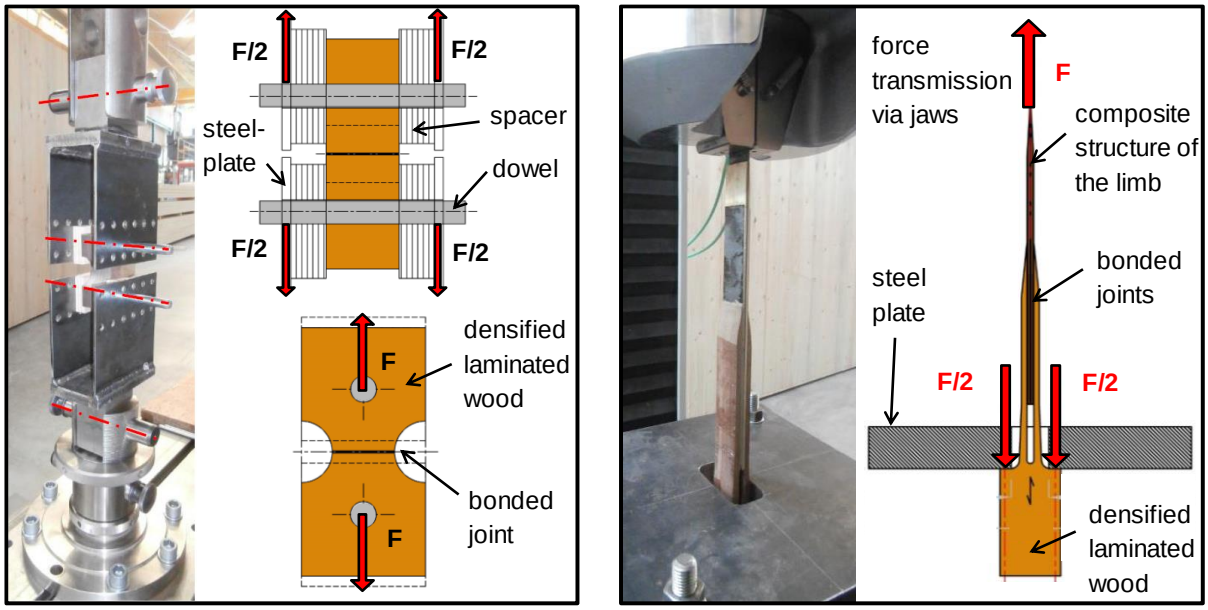

Fig.4: Transverse tensile test Mode I (left) and tensile shear test Mode II (right)

The examination of the tensile opening tests was based on [6] while the plane shear tests bearded on [7]. For both test configurations modifications considering materials, sample geometry, layer structure and load transfer had to be applied in order to better reflect the peculiarities of the bow. The samples were tested under quasi-static conditions with a loading rate of 1.2 mm/min for Mode I and 1.5 mm/min for Mode II. This was in order to achieve the material failure after about 90 seconds. Due to the fact that bows are used over a wide temperature range, the transverse tensile tests were carried out at 20 °C and 80 °C. For the tensile shear tests a reduced test program was used with samples only tested at 20 °C.

3.1.2 Quasi-static loading and dynamic unloading tests

For the quasi-static loading test, the bow was mounted on a moveable sled, while the middle section of the bowstring was fixed (see Fig. 5). The bow was spanned from its pre-strained state to the fully drawn state with a loading rate of 120 mm/min. For measuring the spanning path an off-rope-extensometer was used. Also, two load cells were applied to the test setup to measure the string force and the draw weight of the bow over the whole spanning process.

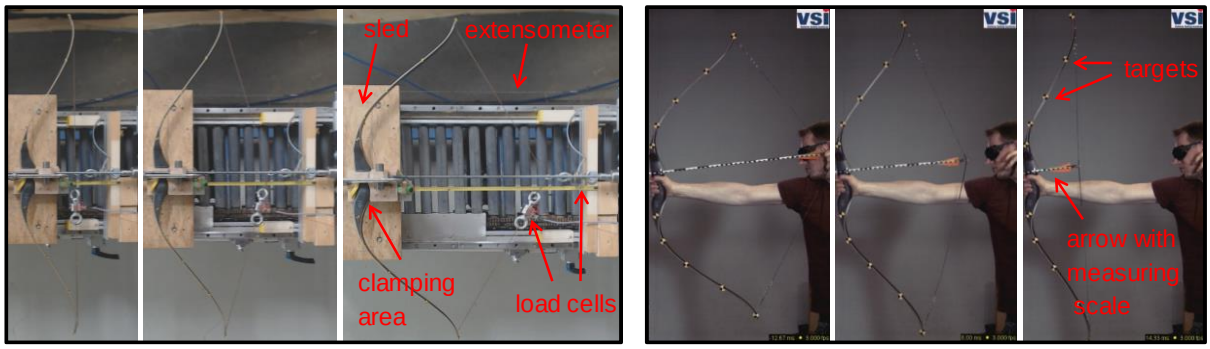

Fig.5: Quasi-static loading test (left) and dynamic unloading tests (right)

The dynamic unloading tests covered the phase between the fully drawn state over the moment when the arrow left the bow up to the oscillation of the system. The launch operation was done manually by an archer and filmed with a high-speed camera. Single sequences from the launching operation are

shown in Fig. 5. To ensure an automated evaluation of the test (target tracking) the bow and the arrow were prepared with targets and measuring scales. Those were necessary to determine the limb kinematics as well as to calculate the arrow velocity.

3.1.3 Dynamic vibration and damping tests

The experiments described in this chapter are basically also dynamic unloading tests. Unlike the launching tests the vibration and damping tests were carried out without arrow and in some configurations even without bowstring. The rationale was to determine the vibration and damping behavior of the simpler system first. Afterwards the observed characteristics should be transferred to the more complex system, which was used in the launching tests. For this test-configuration the bow grip was fixed in a vice as shown in Fig. 6. Furthermore, the end of the lower limb was equipped with an accelerometer to measure the acceleration in local x- and z-direction and test procedure was filmed with a high-speed camera.

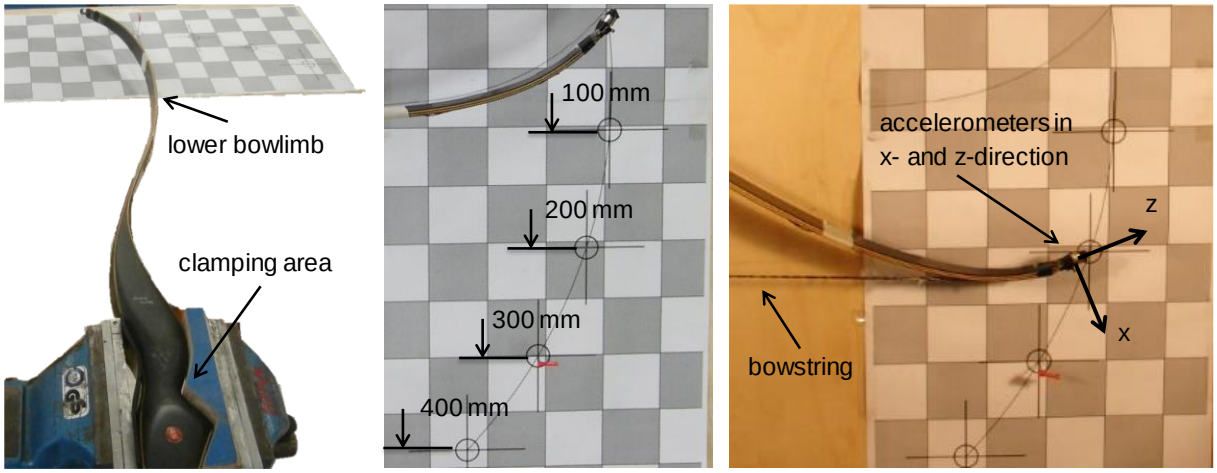

Fig.6: Overview test setup (left), test without bowstring (middle) and test with pre-strained bow (right)

Without bowstring four different deflections ranging from 100 mm to 400 mm were investigated (see Fig. 6). In case of the pre-strained bow the pre-deformation is already 200 mm and only a maximum deflection of 300 mm was tested.

3.2 Numerical tests

In this chapter it is described how the simulation model of the bow with all its individual phases was created. All calculations were carried out with LS-DYNA Version 7.1.1.

3.2.1 3D–Laser scan

The geometry for the numerical model based on the surface data which were obtained by a 3D-Laser scan. The bow was scanned in its unstrung and unloaded initial state with a measurement accuracy of ± 0.01 mm. The result of the 3D-Laser scan was a point cloud with about 4.3 million single points. In a next step a surface model with around 2.5 million areas was triangulated out of the point cloud. Fig. 7 shows one end of a real bow limb compared to the generated point cloud and the surface model.

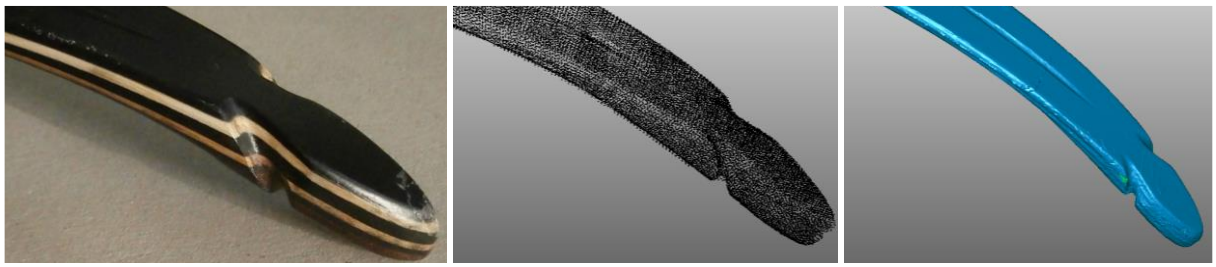

Fig.7: Real bow limb (left), point cloud of the limb (middle) and returned surface model (right)

In order to use the surface model for further modelling steps the limbs were simplified to a 2D structure.

3.2.2 Model features

As already indicated, the composite structure of the limbs was modelled with shell elements and ***Mat_composite_damage** in combination with ***part_composite** (see Fig. 8). Due to the fact that the layer thickness of the limbs is decreasing towards the end, it was subdivided into six individual sections. For the bow grip solid elements and ***Mat_orthotropic_elastic** were used. The laminar limb structure was assigned to the top sheets of the grip on both the compression and the tension side. For modelling the transition zone between limb and grip ***nodal_rigid_bodies** were used.

The string was modelled with beam elements and for the yellow and red sections of the string (see Fig. 8) ***mat_plastic_kinematic** was used. The blue section which was used for the contraction of the string in order to pre-strain the bow was modelled with ***mat_null**. The null beam was included for pulling back the arrow in bracing and drawing. To do so, the rear end of the arrow-nock was closed with a null shell element. Once fully drawn, the contact between this element and the bow-string was deactivated (to allow a free flight of the arrow). For the contact modelling between bowstring and limbs a ***automatic_nodes_to_surface** contact was used. The arrow was modelled with beam elements and ***mat_elastic**. To provide a visibility in the animation shell elements in combination with ***mat_null** were fixed to the arrow by using ***constrained_nodal_rigid_bodies**.

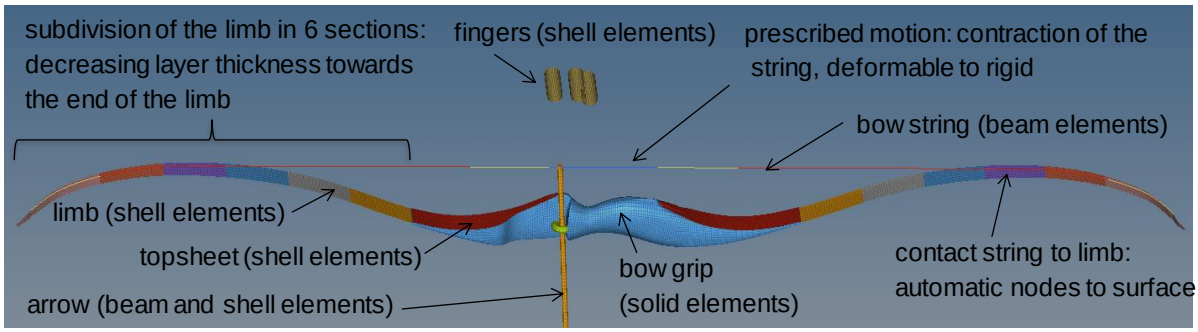

Fig.8: Components and boundaries of the simulation model

Due to the long, slim limbs, the Belychko-Wong-Chang warping stiffness was set to 1 in ***controll_shell**. This was necessary to suppress the twisting of the limbs and getting a realistic stiffness. Furthermore, the laminate theory for shells was activated, which is particularly important for composites with strongly different stiff layers like in the present bow design.

3.2.3 Simulation phases

As already mentioned, the simulation consists of several loading and unloading phases. In the initial state the bow model is unbraced and unloaded which is shown in Fig. 9. The phase between the unbraced and braced situation is called bracing and has a duration of 100 ms. During this phase the bowstring was engaged in order to pre-strain the bow. The next phase between the braced and fully drawn state is called spanning and has also a duration of 100 ms. The fingers of the archer which are modelled with shell elements and ***mat_elastic** were defined to pull the string back to its fully drawn position. In the last phase the stored enery was suddenly released in order to launch the arrow. After nearly 17 ms of acceleration the arrow has left the bow. In order to study the subsequent oscillating phase and the damping behavior of the system the total simulation lasted 500 ms.

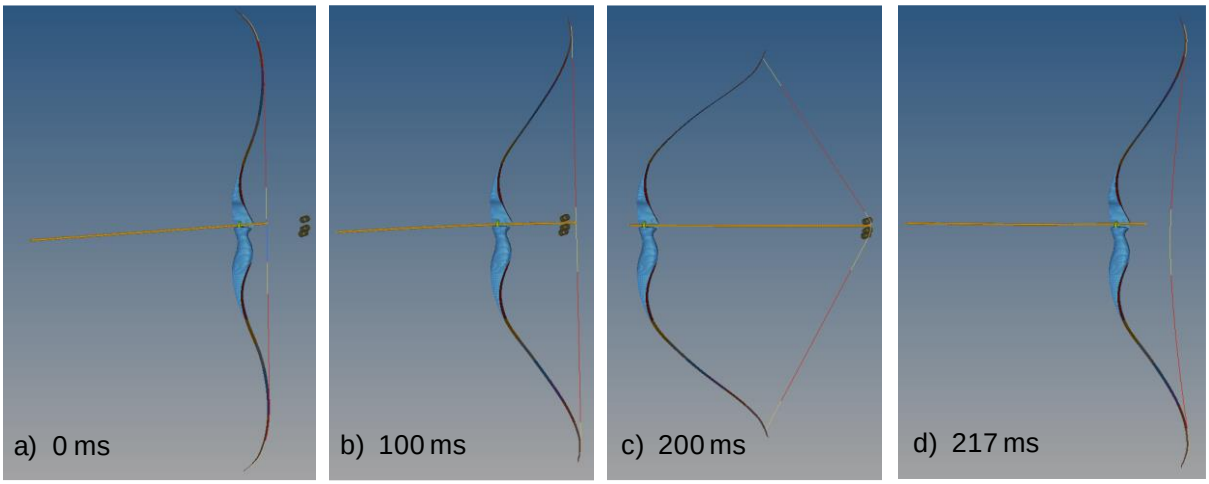

Fig.9: Multiple phases of the bow model: a) unbraced, b) braced, c) fully drawn and d) released

To reach quasi-static conditions (equilibrium) in phases a) through c) `*damping_global` was used. The damping in phase d) was modelled through `*damping_frequency_range`.

3.2.4 Modified sub model I of the bow

To find the ideal settings for `*damping_frequency_range` it was necessary to create a reduced sub model of the bow without arrow and bowstring (see Fig. 10). The sub model was based on the vibration and damping tests and exhibits the same boundary conditions and deflection stages ranging from 100 mm to 400 mm.

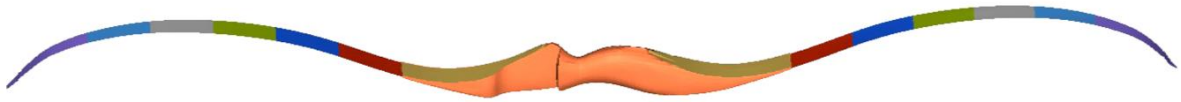

Fig.10: Sub model I without bowstring and arrow

In order to consider the weight of the accelerometers at the end of the limb additional mass was defined in the model. In the first phase the lower limb was deflected with `*boundary_prescribed_motion`. In the second phase the limb was released, and the oscillation phase began.

3.2.5 Modified sub model II of the bow

The submodel II was similar to the overall bow model but without an arrow involved (see Fig. 11). The string consists of many single strains which are twisted together. Therefore, the internal friction between the singe strains plays a major role in the overall damping behavior [8].
Because of the fact that the damping properties of the string are quite different to those of the limbs the damping parameter was adjusted separately for the bow and string such to replicate the free vibration test with and without bow string.

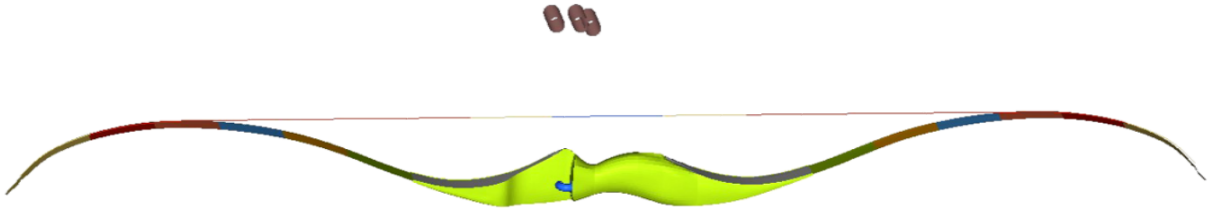

Fig.11: Sub model II with bowstring but without arrow

4 Results

In the course of this chapter, the experimental and numerical results are shown and compared.

4.1 Adhesive properties

In Table 1: the results of the adhesive tests at perpendicular tension are shown. While the tests at 20 °C show an average tensile strength of about 6,3 N/mm² the value dropped to about 0,8 N/mm² at a testing temperature of 80 °C.

test series	number [-]	maximum [N/mm²]	minimum [N/mm²]	mean [N/mm²]	COV [%]
Mode I 20°C	5	8.37	4.22	6.33	27.5
Mode I 80°C	5	1.13	0.521	0.782	27.9

Table 1: Strength properties of the adhesive at perpendicular tension (Mode I)

4.2 Static loading and dynamic unloading behavior

In order to analyze the load level over the individual loading and unloading phases, the bending moment in the transition region between bow limb and grip was calculated (see Fig. 12). In the pre-strained state, the bending moment is already 50 Nm whereas it reached 80 Nm at the fully drawn state. After releasing the arrow there is a sudden decrease of the load level, followed by an oscillation around the level of the pre-strained state. Due to the fact that the highest load level over the whole process is in the fully drawn quasi-static state, the stress analyses in the bow grip were evaluated for this equilibrium condition (see chapter 4.4).

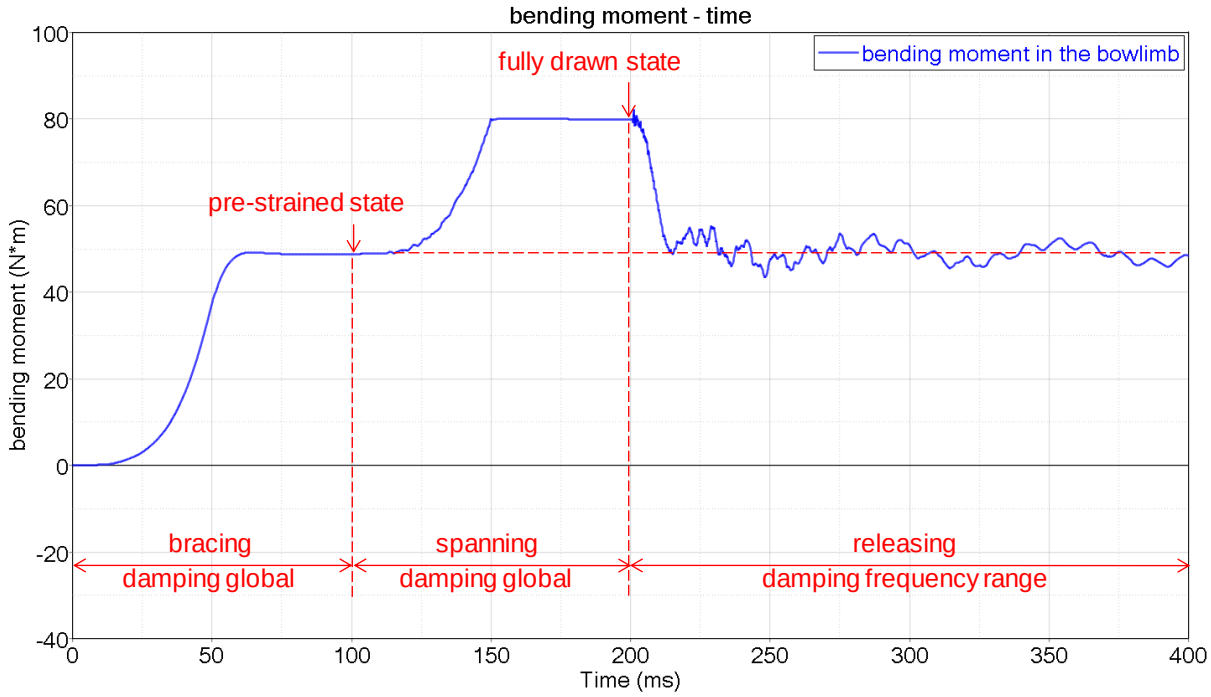

Fig.12: Load level over the simulation phases based on the bending moment in the bow limb

4.3 Vibration and damping behavior

When releasing the bowstring (or just the limb) there is a damped vibration of the system. Fig. 13 shows a comparison of the results from the experimental (grey) and the numerical tests (green and magenta) for the bow without string and a deflection of 200 mm. The acceleration in local x-direction showed a maximum of 550 g and in local z-direction 250 g (after filtering with CFC 180). The range for the damping frequency was defined from 0.02 up to 0.2 ms^{-1} and the damping coefficient was set to 0.01. These settings were obtained from a parameter variation study. The frequency range (FLOW and FHIGH) was selected based on the observed oscillation frequencies.

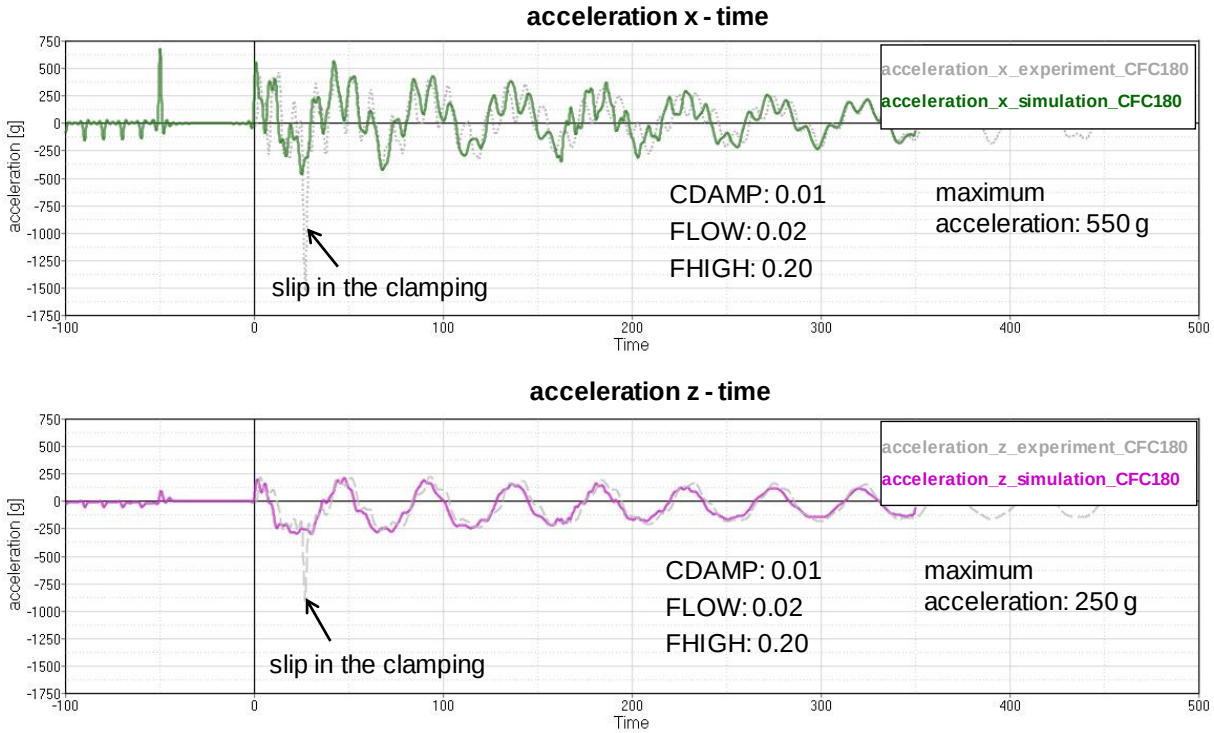

Fig.13: Comparison between sub model I and the vibration tests for 200 mm deflection

For the system with bowstring which is shown in Fig. 14 the damping as well as the acceleration values were significantly higher. The damping coefficient of the string was set to 0.08 while the value for the rest of the bow remained 0.01. The maximum acceleration in local x-direction was about 1000 g whereas the acceleration in local z-direction was nearly 400 g. Because of the pre-strained bow string in the system, the frequency is much higher than in the submodel I. As a result, the damping frequency of this system ranged from 0.05 up to 0.5 ms^{-1}.

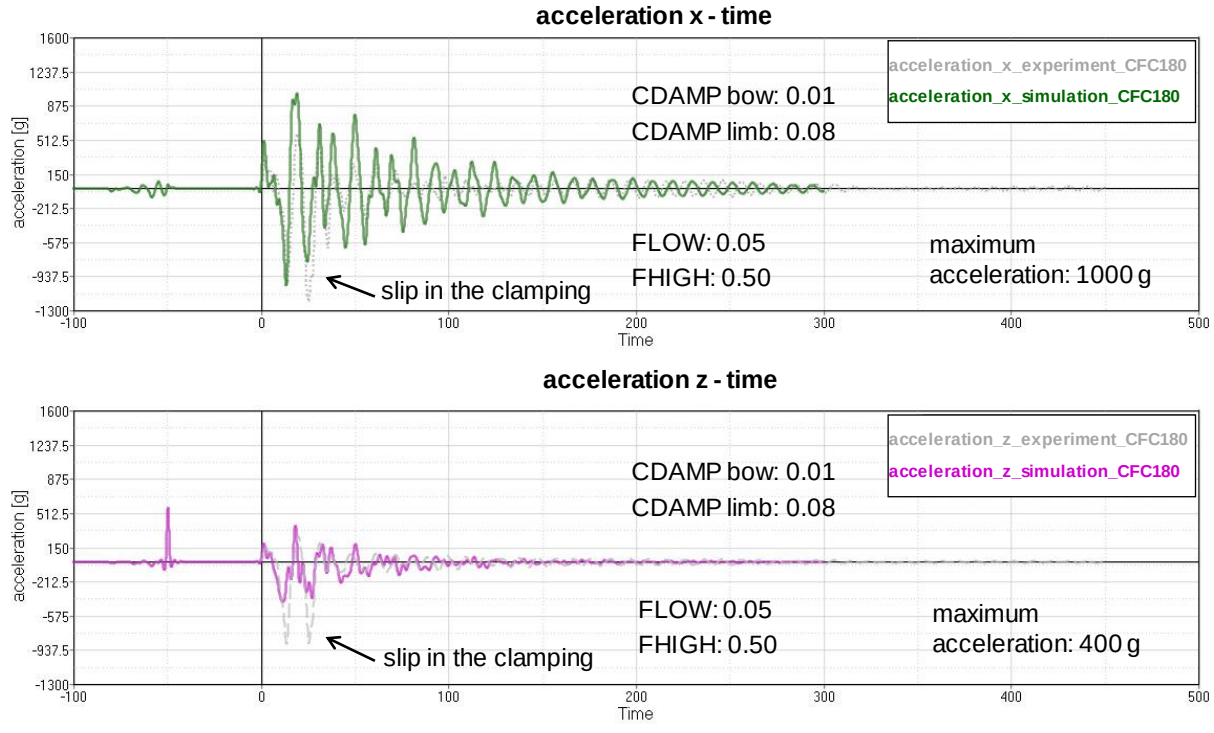

Fig.14: Comparison between sub model II and the vibration tests of the pre-strained bow

4.4 Stress analyses in the bow grip

The evaluation of the stresses in the bow grip concerning normal stresses perpendicular to the grain is shown in Fig. 15. The simulation results show that the highest tensile stresses with 2.8 N/mm² are located in that area of the grip which is rounded inwards. It is the area with the narrowest curvature on the tension side.

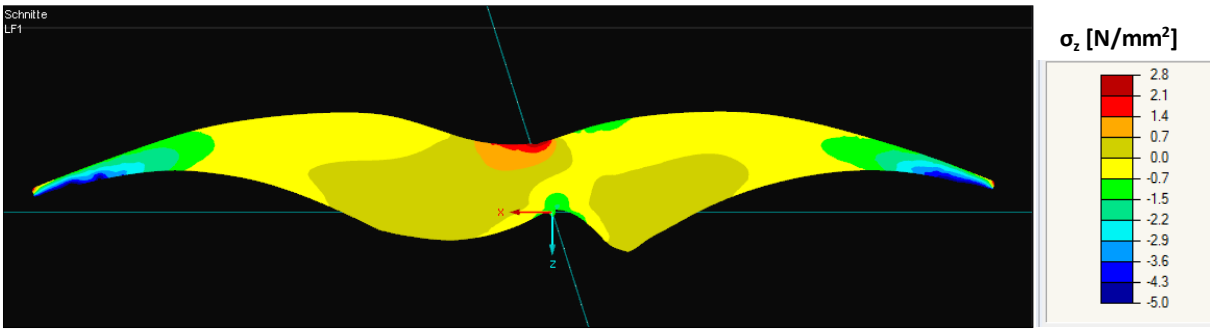

Fig.15: Normal stresses perpendicular to the grain in the bow grip at fully drawn state

Additionally, also the shear stresses in longitudinal direction were evaluated (see Fig. 16). The highest stresses which occur are in the transition region between grip and limbs with about 11 N/mm². In the area of the grip, which is rounded inwards the shear stresses are about 6 N/mm².

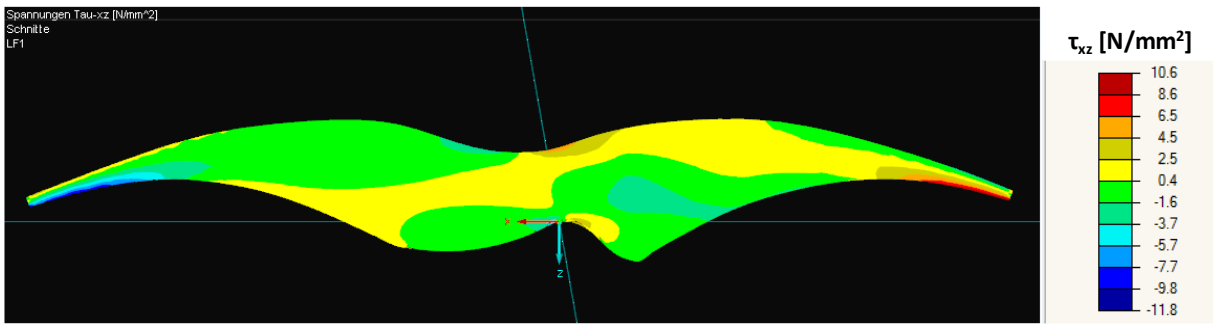

Fig.16: Shear stresses in longitudinal direction in the bow grip at fully drawn state

Because of the fact that the Young's-modulus in perpendicular direction and the shear modulus in longitudinal direction of the grip have almost the same value as the adhesive, it can be assumed that the evaluated stresses in the grip can be directly transmitted to the adjoining adhesive layer.

5 Conclusions

It was shown that quasi-static conditions as well as the post-release damping behavior can be fairly well replicated through various **`*damping`** options provided in LS-DYNA. The unusually high accelerations in the first phase of the experimental oscillation data were probably caused by a slippage in the clamping area. The dynamic simulations covered phenomena like the archer's paradox (bending of arrow when released) very nicely. Both the experiment and the simulation showed a maximum arrow velocity of about 60 m/s. Eventually the stresses in the grip and in the individual plies of the composite shell were evaluated for the fully drawn state and compared against the technical properties (established in experimental tests) of the adhesives. Investigations about a possible cumulative damage during the oscillating phase around the load level of the pre-strained state were not considered.

The experimental tests on the adhesive showed a significant reduction of its strength properties with increasing temperature. The study showed that the combination of several factors leads to the delamination problem in the bow grip. It is assumed that the high service temperature during use on hot summer days together with the high stress level perpendicular to the lamina layers (transverse tension) in interaction with transverse shear was primarily responsible for the delamination failure. Furthermore, additional effects like production induced stresses of the adhesive and also residual stress in the composite layer which were caused by their narrow-curved geometry were probably partly responsible for the failure. These mechanisms are not further discussed in the course of this

work but can be read in [9]. Based on this model minor design changes were suggested to prevent delamination failure in future bow designs but also studying and improving the system as a whole.

6 Literature

[1] Gordon Composites: „Product Secifications GC-70-UCL“, datasheet, 2004, pp. 2, http://www.gordoncomposites.com/products/TDS/GC-70-UCL.pdf | 2017-02-22

[2] Gordon Composites: „Product Secifications GC-70-UL“, datasheet, 2004, pp. 2, http://www.gordoncomposites.com/products/TDS/GC-70-UL.pdf | 2017-02-22

[3] Sharma B., Bauer H., Schickhofer G., Ramage M.: „Mechanical characterisation of structural laminated bamboo“, Proceedings of the Institution of Civil Engineers, 2016, pp. 7, DOI: http://dx.doi.org/10.1680/jstbu.16.00061

[4] Haller P., Heiduschke A., Putzger R., Hartig J.: „Kunstharzpressholz zur Verstärkung von Brettschichtholz“, essay, 2015, pp. 2, DOI: 10.1002 / bate.201400085

[5] KauPo Kautschuk + Polyurethane: „Technisches Merkblatt EA-40®“, datasheet, 2017, pp 1, http://www.kaupo.de/produkte/epoxidkleber/ea-40/ | 2017-07-04

[6] ÖNORM EN 302-3: „Klebstoffe für tragende Holzbauteile – Prüfverfahren Teil 3: Bestimmung des Einflusses von Säureschädigung der Holzfasern durch Temperatur- und Feuchtezyklen auf die Querzugfestigkeit“, Österreichisches Normungsinstitut, 2015-10-15

[7] ÖNORM EN 302-1: „Klebstoffe für tragende Holzbauteile - Prüfverfahren Teil 1: Bestimmung der Längszugscherfestigkeit“, Österreichisches Normungsinstitut, 2013-05-10

[8] Dobes M., Navratil J.: „Damping – Oscillation Elimination after Rupture “, 14. Deutsches LS-Dyna Forum, 2016, pp. 3-5

[9] Baumann G.: „Geometrie- und Spannungsoptimierung eines einteiligen Recurvebogens“, master thesis, 2017, pp. 104-111